# Optical detection of Aflatoxins B in grained almonds using fluorescence spectroscopy and machine learning algorithms

F. R. Bertani[a], L. Businaro[a], L. Gambacorta[b], A.Mencattini[c] , D. Brenda[c], D. Di Giuseppe[c], A. De Ninno[a], M. Solfrizzo[b], E. Martinelli[c], A. Gerardino[a]

[a]Consiglio Nazionale delle Ricerche, Istituto di Fotonica e Nanotecnologie, via Cineto Romano 42, 00156, Roma, Italia

[b] Consiglio Nazionale delle Ricerche, Istituto di Scienze delle Produzioni Alimentari, via Amendola, 122/O - 70126 Bari, Italia

[c]Department of Electronic Engineering, University of Rome Tor Vergata, via del Politecnico 1, 00133, Roma, Italia

e-mail: francesca.bertani@ifn.cnr.it

**Abstract**

Aflatoxins are fungal metabolites extensively produced by many different fungal species that may contaminate a wide range of agricultural food products. They have been studied extensively because of being associated with various chronic and acute diseases, especially immunosuppression and cancer, and their presence in food is strictly monitored and regulated worldwide.

Aflatoxin detection and measurement relies mainly on chemical methods usually based on chromatography approaches, and recently developed immunochemical based assays that have advantages but also limitations, since these are expensive and destructive techniques. Nondestructive, optical approaches are recently being developed to assess presence of contamination in a cost and time effective way, maintaining acceptable accuracy and reproducibility. In this paper are presented the results obtained with a simple portable device for nondestructive detection of aflatoxins in almonds. The presented approach is based on the analysis of fluorescence spectra of slurried almonds under 375 nm wavelength excitation. Experiments were conducted with almonds contaminated in the range of 2.7-320.2 ng/g total aflatoxins B ($AFB_1$ + $AFB_2$) as determined by HPLC/FLD. After applying pre-processing steps, spectral analysis was carried out using a binary classification model based on support vector machine (SVM) algorithm. A majority vote procedure

was then performed on the classification results. In this way we could achieve, as best result, a classification accuracy of 94% (and false negative rate 5%) with a threshold set at 6.4 ng/g. These results illustrate the feasibility of such approach in the great challenge of aflatoxin detection for food and feed safety.

## *1. Introduction*

Aflatoxins are a group of chemically related mycotoxins formed by microscopic fungi (*Aspergillus flavus*, *A*. *parasiticus*, and *A*. *nomius*) occurring in corn, cottonseed, peanuts and other nuts, grains and spices (Eaton and Groopman, 1993; Fao, 2016) Fungal infection and aflatoxin production can occur at any stage of plant growth, harvesting, drying, processing, and storage. Both the infection process and aflatoxin accumulation are strongly affected by environmental conditions such as insect damage, temperature, and humidity. Aflatoxins can contaminate food both before and after harvest and cannot be destroyed by any form of food processing (Rustom, 1997): they occur in more than ten varieties (including B1, B2, G1, and M1 and M2 which are secreted in the milk of lactating animals that have consumed feed contaminated with aflatoxin), aflatoxin B1 being the most prevalent and toxic one (Rasch et al., 2010). Exposure by ingestion or inhalation of aflatoxins may lead to the development of serious medical conditions that vary considerably depending on the animal species, dose, diet, age, and gender (Kumar et al., 2017). Acute effects are primarily observed in structural and functional damage of the liver, including liver cell necrosis, haemorrhage, lesions, fibrosis, and cirrhosis. Additionally, hepatic encephalopathy, immunosuppression, lower respiratory infections, anorexia, malaise, and fever have been observed. It is furthermore considered the most potent naturally occurring carcinogen and is designated group 1 human carcinogen (Eaton and Groopman, 1993; IARC, 1993; Streit et al., 2012).

The maximum permitted levels of aflatoxins in food and feed products are regulated in over 100 nations (Unnevehr and Grace, 2013). The European Commission for example states the maximum allowed total aflatoxin levels in different food materials (Commission Regulation (EC), 2006a), while the USA food safety regulations included a limit of 20 ng/g of total aflatoxins in all food products (FDA, 2000). There are

currently several different accepted measurement techniques available for determining aflatoxin levels (Tittlemeier et al., 2019; Fao, 2016; Ricci et al., 2007). In general, conventional measurement techniques require three steps: extraction with mixture of water and organic solvents; purification to concentrate the extract and remove interferents as much as possible; finally separation, detection and quantification of analytes. Conventional purification techniques are based on solid phase extraction (SPE), a mainstay of analytical chemistry. Examples include, reversed phase- and silica-based SPE columns and immunoaffinity based columns. For separation, detection and quantification high pressure liquid chromatography (HPLC) coupled with fluorescence or mass spectroscopy (MS) detector is mainly used for food and feed analysis whereas thin layer chromatography (TLC) is mainly used in developing countries (Fao, 2016). HPLC based methods are well-proven and widely accepted, however they are laborious, time consuming, require well trained personnel and are costly because they need a significant investment in consumables, equipment and maintenance (CEN-EN, 2007). Some more modern and rapid methods (Yao et al., 2015) are quantitative such as ELISA, or semi-quantitative such as lateral flow tests, direct fluorescence, fluorescence polarization immunoassay and biosensors (Dinçkaya et al., 2011; Eivazzadeh-Keihan et al., 2017). Indirect methods are based on mid- or near-infrared spectroscopy (Kimuli et al., 2018; Pearson et al., 2001; Wu et al., 2018) and do not directly measure aflatoxins but measure an indicator that is associated with the production of aflatoxins. Emerging technologies include hyperspectral imaging (Kalkan et al., 2011; Wang et al., 2015), electronic nose, aptamer-based biosensors (Castillo et al., 2015), molecular imprinted polymers, nanoparticle-based and cell-based approaches (Larou et al., 2013).

Besides being costly, destructive and time consuming, the sample-based analysis often gives a limited view on the degree of contamination if the laboratory sample is not obtained with a correct sampling procedure (Commission Regulation (EC), 2006b; Commission Regulation (EU), 2014). This is due mainly to the inhomogeneity of the toxin distribution in both the food products and the crops. The true aflatoxin level cannot be determined with 100% accuracy, causing difficulties in the segregation of aflatoxin-contaminated food and feed without destroying a large amount of products and incurring significant economic losses (Shanakhat et al., 2018). The already published non-invasive and non-destructive optical (Tao et al., 2018) and fluorescence methods allow the identification of toxins in liquids, like beer or wine, and in grains and

79 nuts (Rasch et al., 2010; Smeesters et al., 2015). In fact, must be considered that fluorescent toxins can be
80 easily identified if no or very low background fluorescent elements are present. Cereals and nuts, as in the
81 results here presented, usually contain various fluorescent proteins which make the aflatoxin detection
82 challenging (Schade and King, 1984). Nevertheless, since aflatoxins are fluorescent substances,
83 fluorescence spectroscopy seems the most promising non-destructive optical detection technique. To
84 detect aflatoxins, recent studies focused on analyzing both one- and two-photon induced fluorescence
85 spectra of healthy and contaminated maize grains (Smeesters et al., 2015) employing huge laboratory
86 instruments (lasers, sensors, etc). Fluorescence polarization immunoassay is portable and can be used at
87 field as semi-quantitative test but it is limited to detecting one mycotoxin at a time (Yao et al., 2015). The
88 dipsticks and lateral flow devices are also portable, disposable and usable in field. These membrane-based
89 kits can provide a qualitative yes/no determination of the presence of aflatoxin or a threshold result in 5-10
90 min. Biosensors like surface plasmon resonance have high selectivity and sensitivity, ease of use, low cost
91 and portability that would allow it to be used in field applications. Most common biosensors developed for
92 detecting aflatoxins are optical or electrochemical (Yao et al., 2015).

93 In our experiments we found that almond matrices show a marked intrinsic fluorescence emission in the
94 observed spectral range. Despite this, AFB detection in the range of concentration analyzed (ng/g) is
95 possible by fluorescence spectra analysis and machine learning algorithms implementation. In this paper
96 preliminary results of fluorescence spectroscopy for the detection of aflatoxin contamination on slurried
97 almonds are presented. In future, the availability of a multispectral, cheap, rapid and non-destructive
98 techniques will represent a real benefit in the field of food safety, especially in developing countries or in
99 rural environments. Detection of mycotoxins in food products is one of the objectives of the PhasmaFOOD
100 project (www.phasmafood.eu), funded by the EU program H2020, that has the objective to develop a
101 multi-sensing platform by the integration of VIS and NIR micro-spectrometers that will serve as actual
102 chemical sensor.

## 2. Material and methods

### *2.1 Production of aflatoxin contaminated almonds*

Shelled almonds (cs. Genco) were inoculated with a strain of *Aspergillus flavus* (ITEM 7828) producing aflatoxins $B_1$ and $B_2$, according to the experimental conditions reported elsewhere (Zivoli et al., 2014). After incubation with *A. flavus*, almonds (1 kg) were dried at 40 °C for 48 hr, ground, homogenized and (3.12 g) mixed with 496.97 g of blank (uncontaminated) ground almonds. The 500 g of contaminated almonds were added with 1000 ml water and slurried for 5 min with a T25 ULTRA-TURRAX (IKA®-Werke GmbH & CO. KG, Staufen im Breisgau, Germany) to obtain ground almonds homogeneously contaminated with aflatoxins. The slurried almond sample was freeze-dried, ground and analysed in triplicate by HPLC-FLD (see below) resulting in $AFB_1$ and $AFB_2$ levels of 290.6 ± 9.0 ng/g and 29.2 ± 1.6 ng/g, respectively. Different aliquots of this contaminated sample were mixed with blank ground almonds to prepare 8 x 80 g of ground almonds containing lower levels of $AFB_1$ and $AFB_2$. The nine (the first highly contaminated and 8 with intermediate contamination levels) contaminated almond samples were each slurried for 5 min with 160 ml water, freeze-dried, ground and analysed by HPLC-FLD to accurately measure the levels of $AFB_1$ and $AFB_2$. Samples of blank ground almond and contaminated ground almonds were then analysed in quadruplicate by fluorescence spectroscopy.

### *2.2 Determination of $AFB_1$ and $AFB_2$ in contaminated almonds*

A validated HPLC-FLD method (Zivoli et al., 2014) was used to accurately measure aflatoxin levels in artificially contaminated samples of ground almonds. In particular, 5 g of dry ground almonds were extracted with 50 ml of a mixture of acetone/water (85:15 v/v) by sonication for 30 min. After filtration on fluted no. 4 filter paper (Whatman), 5 ml of filtered extract was diluted with 75 ml of ultrapure water and filtered with a GF/A glass microfiber filter (Whatman). Forty milliliters of filtered diluted extract (equivalent to 0.25 g of matrix) was passed through the immunoaffinity column AflaTest (Vicam, Milford, MA). The column was then washed twice with 10 ml of ultrapure water, and aflatoxins were eluted with 1.5 ml (3 × 0.5 ml) of methanol. The three methanolic eluates were collected, diluted with ultrapure water up to 5 ml in a volumetric flask, and analyzed by HPLC-FLD. The samples extracts containing high aflatoxin

129 concentration that overloaded the capacity of the immunoaffinity were reanalyzed. In particular, the
130 samples extract was diluted ten times with water and 5 ml were purified as described above.

131 The HPLC-FLD analyses were performed with an Agilent 1260 Infinity (AgilentTechnologies, Inc.,
132 Wilmington, DE, USA) consisting of a binary pump (G1312B), an autosampler (G1367E) with a 100 µl loop, a
133 fluorescence detector (G1321B) fixed at 365 nm $\lambda_{ex}$ and 435 nm $\lambda_{em}$, a column oven (G1316C) set at 30 °C
134 and a software for Microsoft Windows 7 (OpenLAB, CSB, ChemStation Edition). The column used was a 150
135 mm × 4.6 mm i.d., 3 µm, Luna PFP (2) (pentafluorophenyl-propyl) with a 3 mm i.d., 0.45 µm pore size guard
136 filter. The chromatographic separation was performed in the isocratic condition using a mixture of
137 MeCN/$H_2O$ (30:70 v/v) at flow rate of 0.8 ml/min. A photochemical post-column derivatization UVE system
138 (LCTech, Dorfen, Germany) was used to enhance the fluorescence of $AFB_1$. The results of $AFB_1$ and $AFB_2$
139 levels measured in the 9 samples of ground almonds are reported in Table 1.

140 (Table 1)

141 ## 2.3 Rapid fluorescence measurement

142 The experimental dataset has been collected through two different measurement sessions, the first at
143 location 1 (ISPA-CNR laboratories of Bari, Italy) in April 2018, the second at location 2 (Rikilt laboratories in
144 Wageningen, Netherlands) in June 2018.

145 To perform fluorescence spectroscopy measurements, a commercial Hamamatsu micro-spectrometer
146 model C12880MA has been identified for its characteristics of sensitivity and wide spectral range (340-850
147 nm). The spectral resolution for this model is 15 nm. The micro-spectrometer has been mounted in a 90
148 degree configuration with the lighting system, in a optical set-up that ensures a distance of 5 cm from
149 sample surface to spectrometer, since the case containing illumination, detector and control electronic
150 boards is laid with an observation window in contact with the upper edge of the dish containing the sample
151 (Fig. 1).The level of sample inside the Petri dish is arranged to reach the edge, so that the surface of the
152 sample is at a fixed distance from the detector entrance. The detection area, considering numerical
153 aperture of spectrometer (NA=0,22) and the distance between the sample surface and the spectrometer is

154 approximately 10,5 $cm^2$. In this configuration, the measured light intensity in the detection area is 0,3
155 $mW/cm^2$.
156 (Figure 1)
157
158 The illumination system consists of two UV LEDs (Nichia radial 405648, 375 nm wavelength emission,
159 radiant flux typically 7500 μW). Hamamatsu electronic evaluation board and acquisition software have
160 been used to drive the micro-spectrometer and collect the data. In order to avoid saturation effects from
161 excitation light beam reflectance, a longpass plastic sheet filter with 400 nm cut on wavelength has been
162 placed in front of spectrometer entrance slit (39-426 Edmund Optics).
163 To collect fluorescence spectra, integration time has been set at 200 ms and a dark signal acquired with UV
164 excitation light off. To protect the detector from environmental light a non fluorescent and non reflecting
165 black fabric has been put around the case and sample during sample and dark measurements.

166 In order to take into account variability in the measurement procedures, measurements have been
167 acquired in two different laboratories and in different days for each laboratory session: for each of the ten
168 contamination levels (1 non-contaminated amount and 9 other contaminated amounts containing levels of
169 2.7, 4.4, 6.4, 8.9, 10.7, 13.7, 18.3, 45.2, 320.2 ng/g of total aflatoxins), quadruplicate samples have been
170 prepared for each contamination level putting ground almond in 60 mm-diameter Petri dishes (Fig. 2). The
171 Petri dishes containing contaminated and not contaminated almond were analysed in location 1 and
172 successively in location 2. Notably, in the two measurement sessions (locations 1 and 2), the same almond
173 samples were used, while two different measuring instruments were adopted that included same model
174 elements (C12880MA spectrometer and Nichia LEDs) in approximately the same optical configuration. UV-
175 excited fluorescence spectra have been recorded in five different spatial positions over each sample, and
176 for each position five replicates have been acquired and averaged.To summarize, in location 1 we collected
177 100 measurements (i.e., a quadruplicate sample acquired in 5 positions for 5 replicates) a day for each
178 contamination level and the non contaminated samples: the total number of measures for two days hence

corresponds to 2000 measures in total. For location 2, we collected data for three days obtaining 3000 measures. The whole dataset is hence composed by 5000 measures.

(Figure 2)

## 2.4 Data analysis

The data analysis process has been divided into two phases: a preliminary analysis made of a set of pre-processing steps, and the classification procedure. A schematic picture of the method is shown in Fig.3. All the simulations have been performed in Matlab 2018b.

(Figure 3)

The preliminary analysis has been structured into a set of pre-processing steps, whose main target was to build the two datasets (one for each measurement session) and to identify the optimal threshold value for class definition purpose. In Fig. 4, the spectrum of 18.3 ng/g samples is shown and a peak at about 410 nm is present, due to the not totally filtered excitation reflectance signal. This peak is present in all the collected spectra and represents a common characteristic of all the data.

(Figure 4)

Collected data resulted to have a moderate reproducibility between-day (see Fig. 4) and a relevant dispersion of data. This effect is mainly due to the differences in the experimental setups (due to little differences in the geometrical arrangement of the sensor and illumination in the 2 prototypes). During the data analysis phase, to properly extract the information contained in the spectra and to create appropriate datasets, a feature selection and normalization strategy for fluorescence spectra was applied. In the proposed strategy, in order to select features, we computed the Area Under the Receiving Operating Characteristic (ROC) Curve (AUC) score (Bradley, 1997) for each spectrum dataset with respect to the corresponding reference contamination level. The procedure is applied on the training set. The AUC is computed for each spectrum value and features exhibiting AUC values higher than 0.6 are then selected and used also in the testing set. The limit value has been chosen within the range [0.5-1] as a trade off

between a too strong feature reduction and the selection of not significant features. Normalization has been performed by standard autoscaling (Mclachlan, 1992).

For the classification task, we applied a Support Vector Machine (SVM) algorithm with Radial Basis Function (RBF) kernel to the binary classification problem of safe vs contaminated samples (C. Bishop, 2009). For SVM hyperparameters, we used the Matlab default setting for RBF kernel corresponding to a box constrained value equal to 1, kernel autoscaling, and value of gamma parameter equal to 0.1.

During optimization process, we considered different threshold values between 2.7 and 13.7ng/g. The range has been chosen according to the EU regulation limits (8-10 ng/g in the case of almond(CEN-EN, 2007)). For each threshold value $TH$, we define the two classes $C_1$ and $C_2$ as

$$C_1 \rightarrow L_{cont.} \leq TH$$

$$C_2 \rightarrow L_{cont.} > TH$$

Where $L_{cont.}$ represents the actual contamination level of the considered sample, while $TH$ represents the threshold value. Independent dataset testing has been implemented by using a location for training and the other location for testing and viceversa.

Standard classification approach has been also supported by a majority voting procedure applied to the labels (classification results) assigned to the spectra acquired on samples with the same contamination level and in different spatial positions (see par. 2.2). In such a way, the approach exhibits increased robustness to heterogeneity of the sample contamination that may occur.

The parameters used to evaluate the goodness and the reliability of each result are represented by prediction accuracy. We define as instance the result of a measurement (fluorescence spectrum). The notation used to indicate the four types of instances within the confusion matrix is the following:

- TP (True Positive) → Highly contaminated instances that have been classified properly
- TN (True Negative) → NOT contaminated instances that have been classified properly

- FN (False Negative) → Highly contaminated instances that have been classified as NOT contaminated
- FP (False Positive) → NOT contaminated instances that have been classified as highly contaminated

According to this notation, the classification accuracy (ACC) can be calculated as follows:

$$ACC = \frac{TP + TN}{TP + TN + FN + FP}$$

Table 2 shows the accuracy values (ACC) and the False Negative Rate (FNR) (i.e., the number of false negatives achieved divided by the total number of positive instances, TP+FN) for the two locations: "Location 1" means that the data collected in location 1 have been used as test and the data collected in location 2 has been used as training data, Location 2 is the reverse case. The first column shows the fixed contamination threshold; the next two columns display ACC and FNR obtained for training data set; the last four columns list the ACC and FNR for testing data set before and after the implementation of the majority voting procedure on the instances coming from samples with the same contamination level.

(Table 2)

## Results and Discussion

The FNR value is crucial in food contamination analysis where the risk associated to a false negative instance (contaminated sample misclassified as safe) is higher than the risk of a false positive instance (safe sample misclassified as contaminated). Numbers in brackets represent the balanced accuracy values computed as the average value of the True Positive Rate (TPR) and of the True Negative Rate (TNR). As expected balanced accuracy values are in general lower and account for data unbalancing between the two classes. The optimal threshold value represents a trade-off condition. When the threshold value is low many more samples are assigned to the contaminated class. This situation may affect the performance of the training step and the model construction. As a consequence, the model is capable to better recognize contaminated rather than safe samples and the number of FNRs reduces. When the threshold value is high, a few samples are assigned to the contaminated category. Model capability to recognize contaminated

samples reduces and also FNRs increase. Overall, the accuracy values obtained take into account both FNRs and FPRs and, as a consequence, represents a balancing of such kind of errors.

The results reported in Tab. 2 gives evidence to diverse considerations. First of all, location1 and location2 experiments present, as above discussed, a moderate reproducibility in spectra, here represented by the different performance results. In particular, model trained on location 1 better recognizes contamination effects in dataset collected in location 2 (accuracy up to 0.94) with respect to the model trained on data acquired on location 2 (accuracy up to 0.88). These results show heterogeneity of the data acquired at different locations but at the same time the capability of the system to classify samples in challenging real-life conditions with good performance. The main spectral difference is due to little discrepancies in the geometrical arrangement of the setup because in one of the two prototypes used to acquire data (the one used in location 1), other optical and electronic components have been added in the same case for other experiments, possibly influencing optical or electronic readout. Another possible reason for differences are local conditions (power supply stability among others) that could have affected response collection. Intrinsic limitations in the reproducibility of the signal coming from spectrometer and quantified in 10-15% is a source of noise affecting training phase. In addition to these factors, it is worth to note an effect of the improvement of the measurement procedure that became more stable and reproducible day by day during of measurement sessions. Hence, all the mentioned effects produce a difference of the two training datasets that reflects in a difference learning capability of the two classification models. To further support these considerations, we also included Principal Component Analysis (PCA) results of the datasets in terms of locations, days, and contaminations levels in Supplementary documents (see Figure S1).

Secondly, the heterogeneity of the spectra acquired at different positions in samples with the same average contamination is partially encompassed by the majority voting strategy that produces an increase in the accuracy value and an acceptable decrease in the FNRs except for the threshold value of 10.7 ng/g. Beyond the previous considerations, an important result is the demonstration of the feasibility to select a unique threshold value for the classification of contaminated/safe samples (binary classification model). The best results in terms of accuracy (94%) and false negative rate (5%) have been achieved using the location 2

dataset as test and location 1 data set as training and a threshold equal to 6.4 ng/g. This result must be framed in the specific experimental conditions in which the data have been collected: the reference samples have been prepared accordingly to standardised protocols and are quite homogeneous in granularity. The number of spectra acquired per sample are in the range of thousands, also if different locations have been included. The same kind of analysis must be performed on a more populated data set and in "real setting" conditions to prove its effective feasibility.

As an explicative example, fixing the threshold value to 4.4 ng/g (indicating as contaminated samples the ones having a concentration of aflatoxin strictly larger than 4.4ng/g), the method results in an accuracy value of 0.85 and 0.89 for the two locations respectively. Correspondingly, we obtained an FNR of 0 and 0.0476 respectively for locations 1 and 2 that correspond to less than 5% of contaminated instances classified as non contaminated.

(Figure 5)

We represent in Fig. 5 the labels assigned over the original target concentration for the location 1 (Fig. 5 a) and location 2 (Fig. 5 b) after the application of majority voting grouped by sample. The blue curves represent the actual aflatoxin concentration of the sample. The red dashed curves represent the scaled label assigned to the sample. The green line indicates the threshold limit of 4.4 ng/g. All the values are represented in logarithmic scale ($\log(conc + 1)$) to improve visibility. Cyan and black markers locate the FP and the FN samples respectively. As it can be noted, in experiment a) there are not any FN samples while there are 12 FP samples. In experiment b) there are only 4 FN samples ad 9 FP samples. In particular, FN samples (black markers) exhibit concentrations equal to 6.4 ng/g and 8.9 ng/g that are relatively close to the threshold limit. Measurement protocol progressively improved as long as measurement session went on. Hence, test performed on day 1 at location 1 may presents lower performance than test performed on day 3 at location 2, as indicated also by the FPs distribution highlighted in Figure 5.

## Conclusion

The preliminary data here reported allow us to be confident on the capability of fluorescence approach to detect aflatoxin contamination. In this paper, a binary classification model based on SVM algorithm with

Radial Basis Function kernel has been applied after a set of pre-processing steps to select the significant features from the data sets. Moreover, a majority vote procedure has been performed on the classification results coming from spectra acquired on samples with the same reference contamination and acquired in different spatial positions on the same sample. It must be underlined that the analysed data have been collected during two different measurement sessions performed in two different locations and with different instruments, but on the same set of samples. The outcome of the performed analysis is quite encouraging: we could fix a threshold value in the contamination level and assign the measured spectra to the contaminated/non contaminated labels with an accuracy of more than 70% in all the considered conditions.

Anyway, the process of analysis in all its complexity has allowed to identify also the main criticalities of the method used, opening the way to of potential improvements and further developments, the creation of new models taking into account the possible non-uniformity of the natural contamination levels, the employment of the same standardized instrument for all the measures in order to reduce data dispersion.

The proposed spectroscopic technique together with the machine learning analysis shows a great potential and may already represent a helpful approach in developing countries where rapid and low cost contamination testing would be of great benefit (Shephard and Gelderblom, 2014). Importantly, the reported results have been obtained in a very simple set-up in which no focusing of the excitation light has been applied and no specific sample preparation for the analysis needed.

The described results, while quite preliminary, demonstrate the potentiality of such integrated approach to develop a simple and portable device for food safety assessment. The general interest in smart devices often combined with smartphones is confirmed by recent literature (Hossain et al., 2016; Wilkes et al., 2017) and the development of real time, low cost and easy to use food sensors is of great importance both for end users and for developing countries. Further optical and analytical integration of fluorescence emission and visible reflectance spectra with NIR reflectance spectra, as planned in developing PhasmaFOOD project, will allow a more detailed description of contaminants presence and could enable also shelf life prediction for fresh food (Tsakanikas et al., 2018).

**Acknowledgements**. We acknowledge funding from the EU project PhasmaFOOD (contract n. 732541). Yannick Weesepoel, Judith Mueller-Maatsch and Martin Alewijn at Rikilt laboratories for their support in data acquisition. We thank Dr. F. Epifani for preparing the almond culture material inoculated with *A. flavus* at CNR-ISPA laboratories.

Bibliography

Bradley, A.P., 1997. The use of the area under the ROC curve in the evaluation of machine learning algorithms. Pattern Recognit. 30, 1145–1159. https://doi.org/10.1016/S0031-3203(96)00142-2

Castillo, G., Spinella, K., Poturnayová, A., Šnejdárková, M., Mosiello, L., Hianik, T., 2015. Detection of aflatoxin B 1 by aptamer-based biosensor using PAMAM dendrimers as immobilization platform. Food Control 52, 9–18. https://doi.org/10.1016/j.foodcont.2014.12.008

CEN-EN, 2007. CEN - EN 14123 - Foodstuffs - Determination of aflatoxin B1 and the sum of aflatoxin B1, B2, G1 and G2 in hazelnuts, peanuts, pistachios, figs, and paprika powder - High performance liquid chromatographic method with post-column derivatisation and immunoa [WWW Document]. CEN-EN 14123. URL https://standards.globalspec.com/std/1080210/EN 14123 (accessed 7.25.19).

Commission Regulation (EC), 2006a. EUR-Lex - 02006R1881-20180319 - EN - EUR-Lex [WWW Document]. Comm. Regul. No 1881/2006 19 December 2006 Doc. 02006R1881-20180319. URL https://eur-lex.europa.eu/legal-content/EN/TXT/?uri=CELEX:02006R1881-20180319 (accessed 7.25.19).

Commission Regulation (EC), 2006b. Laying down the methods of sampling analysis for the official control of the levels of mycotoxins in foodstuff.

Commission Regulation (EU), 2014. Methods of sampling of large lots, spices and food supplements,

performance criteria for T-2, HT-2 toxin and citrinin and screening methods of analysis Text with EEA relevance - Publications Office.

Dinçkaya, E., Kınık, Ö., Sezgintürk, M.K., Altuğ, Ç., Akkoca, A., 2011. Development of an impedimetric aflatoxin M1 biosensor based on a DNA probe and gold nanoparticles. Biosens. Bioelectron. 26, 3806–3811. https://doi.org/10.1016/J.BIOS.2011.02.038

Eaton, D.L., Groopman, J.D., 1993. The Toxicology of aflatoxins : human health, veterinary, and agricultural significance, 1st ed. Academic Press.

Eivazzadeh-Keihan, R., Pashazadeh, P., Hejazi, M., de la Guardia, M., Mokhtarzadeh, A., 2017. Recent advances in Nanomaterial-mediated Bio and immune sensors for detection of aflatoxin in food products. TrAC Trends Anal. Chem. 87, 112–128. https://doi.org/10.1016/J.TRAC.2016.12.003

Fao, 2016. JOINT FAO/WHO EXPERT COMMITTEE ON FOOD ADDITIVES Eighty-third meeting.

FDA, 2000. Guidance for Industry: Action Levels for Poisonous or Deleterious Substances in Human Food and Animal Feed | FDA [WWW Document]. URL https://www.fda.gov/regulatory-information/search-fda-guidance-documents/guidance-industry-action-levels-poisonous-or-deleterious-substances-human-food-and-animal-feed#afla (accessed 8.2.19).

Hossain, M.A., Canning, J., Cook, K., Jamalipour, A., 2016. Optical fiber smartphone spectrometer. Opt. Lett. 41, 2237. https://doi.org/10.1364/OL.41.002237

IARC, 1993. IARC Monographs on the evaluation of carcinogenic risks to humans vol 56.

Kalkan, H., Beriat, P., Yardimci, Y., Pearson, T.C., 2011. Detection of contaminated hazelnuts and ground red chili pepper flakes by multispectral imaging. Comput. Electron. Agric. 77, 28–34. https://doi.org/10.1016/J.COMPAG.2011.03.005

Kimuli, D., Wang, W., Lawrence, K.C., Yoon, S.-C., Ni, X., Heitschmidt, G.W., 2018. Utilisation of visible/near-infrared hyperspectral images to classify aflatoxin B1 contaminated maize kernels. Biosyst. Eng. 166,

150–160. https://doi.org/10.1016/J.BIOSYSTEMSENG.2017.11.018

Kumar, P., Mahato, D.K., Kamle, M., Mohanta, T.K., Kang, S.G., 2017. Aflatoxins: A Global Concern for Food Safety, Human Health and Their Management. Front. Microbiol. 07, 2170. https://doi.org/10.3389/fmicb.2016.02170

Larou, E., Yiakoumettis, I., Kaltsas, G., Petropoulos, A., Skandamis, P., Kintzios, S., 2013. High throughput cellular biosensor for the ultra-sensitive, ultra-rapid detection of aflatoxin M1. Food Control 29, 208–212. https://doi.org/10.1016/J.FOODCONT.2012.06.012

Mclachlan, G.J., 1992. Discriminant Analysis and Statistical Pattern Recognition.

Pearson, T.C., Wicklow, D.T., Maghirang, E.B., Xie, F., Dowell, F.E., 2001. DETECTING AFLATOXIN IN SINGLE CORN KERNELS BY TRANSMITTANCE AND REFLECTANCE SPECTROSCOPY.

Rasch, C., Kumke, M., Löhmannsröben, H.-G., 2010. Sensing of Mycotoxin Producing Fungi in the Processing of Grains. Food Bioprocess Technol. 3, 908–916. https://doi.org/10.1007/s11947-010-0364-y

Ricci, F., Volpe, G., Micheli, L., Palleschi, G., 2007. A review on novel developments and applications of immunosensors in food analysis. Anal. Chim. Acta 605, 111–129. https://doi.org/10.1016/J.ACA.2007.10.046

Rustom, I.Y.S., 1997. Aflatoxin in food and feed: occurrence, legislation and inactivation by physical methods. Food Chem. 59, 57–67. https://doi.org/10.1016/S0308-8146(96)00096-9

Schade, J.E., King, A.D., 1984. Fluorescence and Aflatoxin Content of Individual Almond Kernels Naturally Contaminated with Aflatoxin. J. Food Sci. 49, 493–497. https://doi.org/10.1111/j.1365-2621.1984.tb12449.x

Shanakhat, H., Sorrentino, A., Raiola, A., Romano, A., Masi, P., Cavella, S., 2018. Current methods for mycotoxins analysis and innovative strategies for their reduction in cereals: an overview. J. Sci. Food Agric. 98, 4003–4013. https://doi.org/10.1002/jsfa.8933

397 Shephard, G.S., Gelderblom, W.C.A., 2014. Rapid testing and regulating for mycotoxin concerns: a
398 perspective from developing countries. World Mycotoxin J. 7, 431–437.
399 https://doi.org/10.3920/WMJ2013.1682

400 Smeesters, L., Meulebroeck, W., Raeymaekers, S., Thienpont, H., 2015. Optical detection of aflatoxins in
401 maize using one- and two-photon induced fluorescence spectroscopy. Food Control 51, 408–416.
402 https://doi.org/10.1016/J.FOODCONT.2014.12.003

403 Streit, E., Schatzmayr, G., Tassis, P., Tzika, E., Marin, D., Taranu, I., Tabuc, C., Nicolau, A., Aprodu, I., Puel, O.,
404 Oswald, I.P., Streit, E., Schatzmayr, G., Tassis, P., Tzika, E., Marin, D., Taranu, I., Tabuc, C., Nicolau, A.,
405 Aprodu, I., Puel, O., Oswald, I.P., 2012. Current Situation of Mycotoxin Contamination and Co-
406 occurrence in Animal Feed—Focus on Europe. Toxins (Basel). 4, 788–809.
407 https://doi.org/10.3390/toxins4100788

408 Tao, F., Yao, H., Hruska, Z., Burger, L.W., Rajasekaran, K., Bhatnagar, D., 2018. Recent development of
409 optical methods in rapid and non-destructive detection of aflatoxin and fungal contamination in
410 agricultural products. TrAC Trends Anal. Chem. 100, 65–81.
411 https://doi.org/10.1016/J.TRAC.2017.12.017

412 Tittlemier, S. A., Cramer, B., Dall'Asta, C., Iha, M. H., Lattanzio, V. M. T., Malone, R. J., C. Maragos, M.
413 Solfrizzo, M. Stranska-Zachariasova & Stroka, J. (2019). Developments in mycotoxin analysis: an
414 update for 2017-2018. World Mycotoxin Journal, 2019; 12 (1): 3-29.

415 Tsakanikas, P., Fengou, L.-C., Manthou, E., Lianou, A., Panagou, E.Z., Nychas, G.-J.E., 2018. A unified spectra
416 analysis workflow for the assessment of microbial contamination of ready-to-eat green salads:
417 Comparative study and application of non-invasive sensors. Comput. Electron. Agric. 155, 212–219.
418 https://doi.org/10.1016/J.COMPAG.2018.10.025

419 Unnevehr, L., Grace, D., 2013. Aflatoxins - finding solutions for improved food safety.
420 https://doi.org/10.2499/9780896296763

421 Wang, W., Ni, X., Lawrence, K.C., Yoon, S.-C., Heitschmidt, G.W., Feldner, P., 2015. Feasibility of detecting
422 Aflatoxin B1 in single maize kernels using hyperspectral imaging. J. Food Eng. 166, 182–192.
423 https://doi.org/10.1016/J.JFOODENG.2015.06.009

424 Wilkes, T.C., McGonigle, A.J.S., Willmott, J.R., Pering, T.D., Cook, J.M., 2017. Low-cost 3D printed 1 nm
425 resolution smartphone sensor-based spectrometer: instrument design and application in ultraviolet
426 spectroscopy. Opt. Lett. 42, 4323. https://doi.org/10.1364/OL.42.004323

427 Wu, Q., Xie, L., Xu, H., 2018. Determination of toxigenic fungi and aflatoxins in nuts and dried fruits using
428 imaging and spectroscopic techniques. Food Chem. 252, 228–242.
429 https://doi.org/10.1016/J.FOODCHEM.2018.01.076

430 Yao, H., Hruska, Z., Di Mavungu, J.D., 2015. Developments in detection and determination of aflatoxins.
431 World Mycotoxin J. 8, 181–191. https://doi.org/10.3920/WMJ2014.1797

432 Zivoli, R., Gambacorta, L., Perrone, G., Solfrizzo, M., 2014. Effect of Almond Processing on Levels and
433 Distribution of Aflatoxins in Finished Products and Byproducts. J. Agric. Food Chem. 62, 5707–5715.
434 https://doi.org/10.1021/jf5018548

435

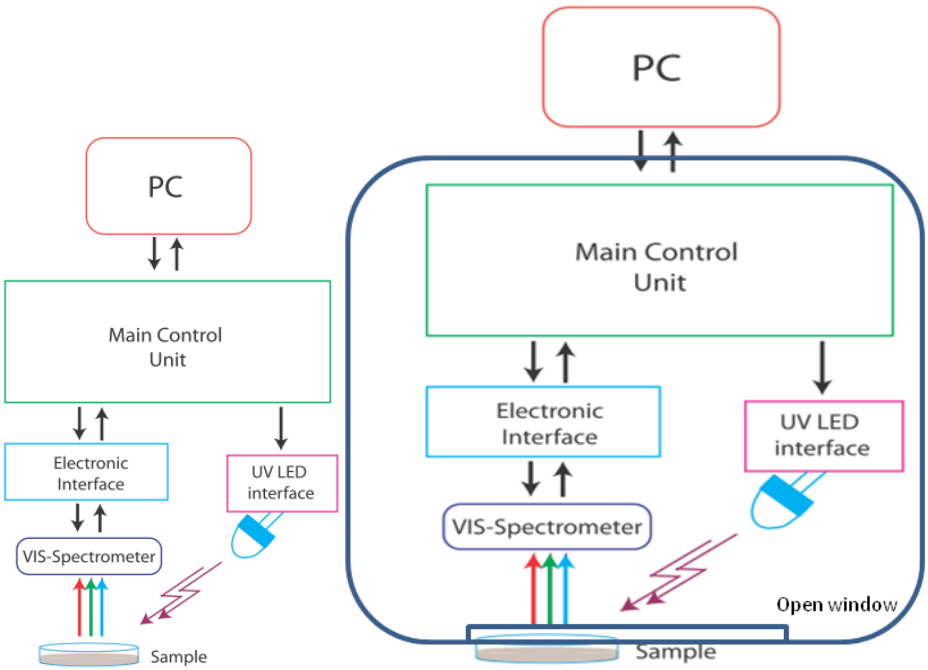


Figure 1 Scheme of the fluorescence spectroscopy set-up.

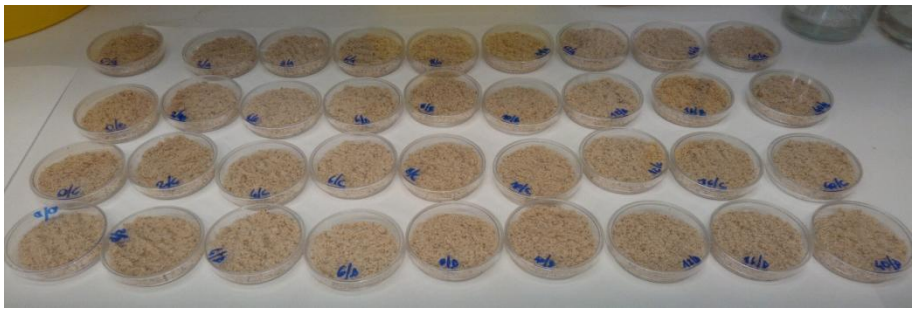

Figure 2: Set of samples. In the figure the level from 0 to 45.6 ng/g are shown in quadruplicate.

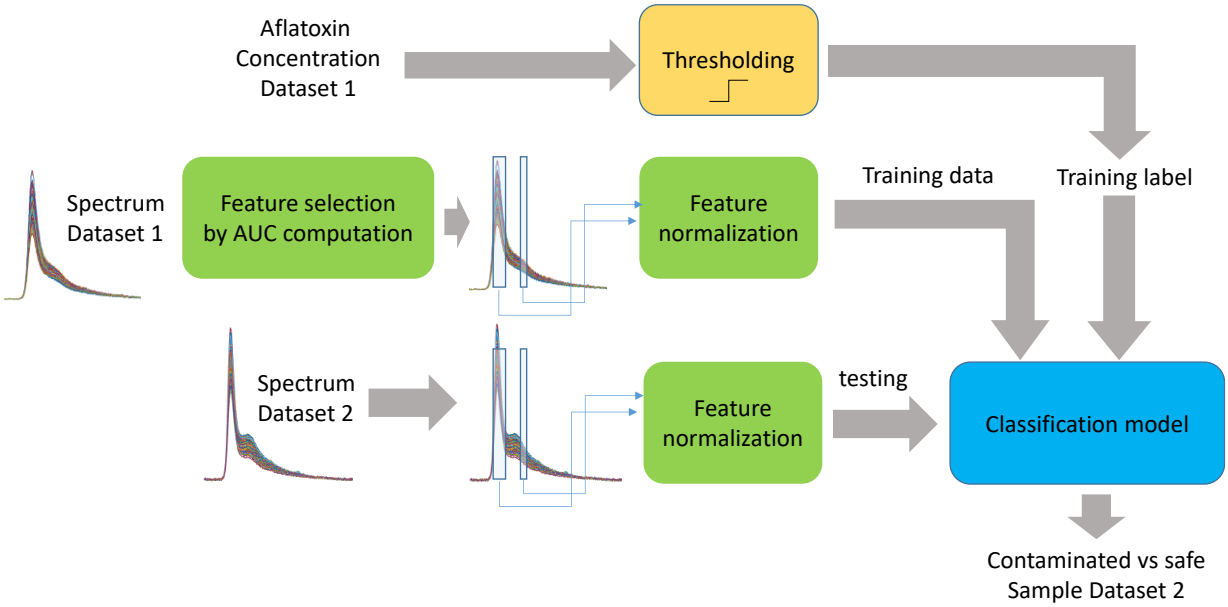


Figure 3. A schematic flowchart of the whole method for the data analysis. Spectrum dataset 1 is used for feature selection. Selected features are all normalized in training and testing by autoscaling. The reference value of aflatoxin is

then thresholded in order to assign a label to the training features of safe (0) vs contaminated (1). The selected level for thresholding is the same for training and testing dataset. A classification model is then constructed on the training set and applied to the testing dataset for sample recognition. The classification step includes a majority voting procedure aimed at performing the majority voting procedure among labels assigned to the testing dataset.

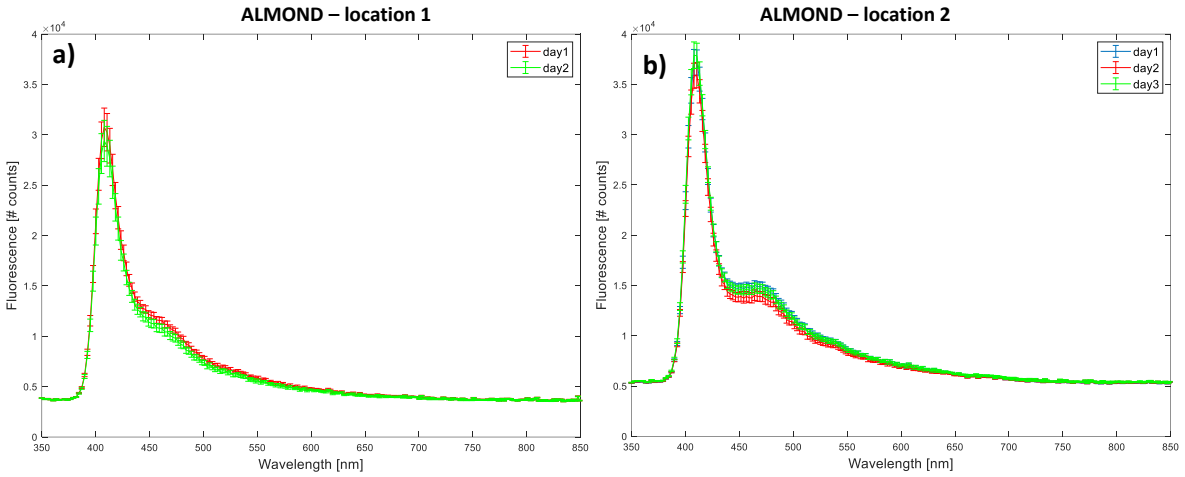


Figure 4. Data collected in location 1 (a) and location 2 (b) (different instruments) in different days on the same sample (18.3 ng/g). Mean and standard deviation values over the same samples are shown. Similar behavior is shown by the fluorescence spectra collected on the other samples.

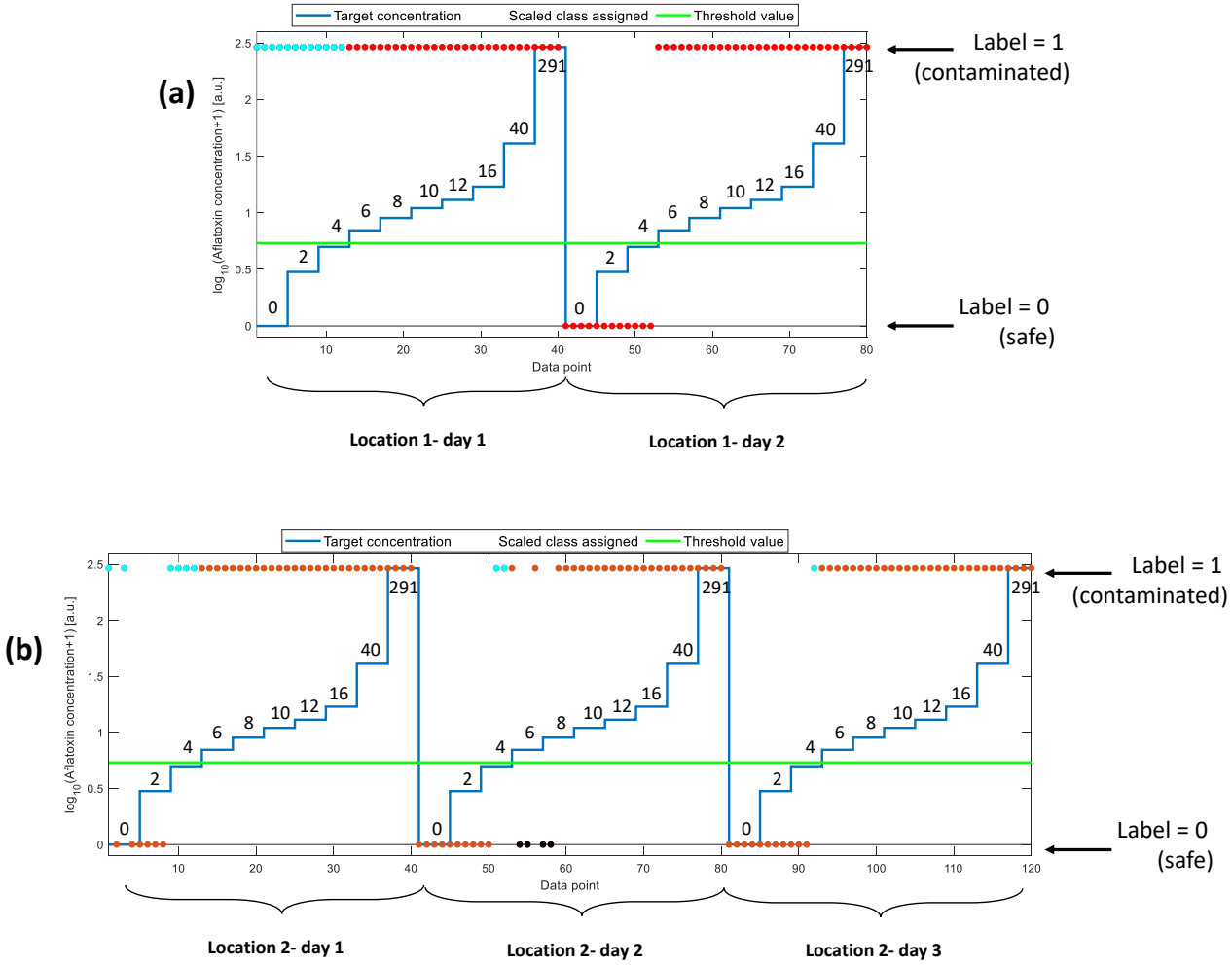


Figure 5. (a) Test at location1 (b) Test at location 2. Blue curves represent the target concentrations. The dashed red curves represent the scaled label assigned by the classifier. The green line is the threshold limit set at 4.4 ng/g. All the

values are represented in logarithmic scale for the sake of visibility and grouped after majority voting by sample (and not by point of acquisition). Cyan markers locate the FP samples and black markers identify the FN samples.

| Sample | $AFB_1$ (ng/g) | $AFB_2$ (ng/g) | $AFB_1$+$AFB_2$ (ng/g) |
|---|---|---|---|
| Almond 1 (control, uncontaminated) | ND | ND | - |
| Almond 2 | 291.0 ± 8.7 | 29.2 ± 1.5 | 320.2 ± 8.9 |
| Almond 3 | 39.3 ± 1.2 | 5.9 ± 0.3 | 45.2 ± 1.2 |
| Almond 4 | 16.4 ± 0.5 | 1.9 ± 0.1 | 18.3 ± 0.5 |
| Almond 5 | 12.5 ± 0.4 | 1.2 ± 0.06 | 13.7 ± 0.4 |
| Almond 6 | 9.9 ± 0.3 | 0.8 ± 0.04 | 10.7 ± 0.3 |
| Almond 7 | 8.3 ± 0.2 | 0.6 ± 0.03 | 8.9 ± 0.3 |
| Almond 8 | 6.0 ± 0.2 | 0.4 ± 0.02 | 6.4 ± 0.2 |
| Almond 9 | 4.2 ± 0.1 | 0.2 ± 0.01 | 4.4 ± 0.1 |
| Almond 10 | 2.6 ± 0.1 | 0.1 ± 0.01 | 2.7 ± 0.1 |

Table 1. Levels of $AFB_1$ and $AFB_2$ in samples of ground almonds used in this study. ND: not detected (LOD 0.2 ng/g)

| | Threshold (ng/g aflatoxins | ACC training | FNR training | ACC testing | FNR testing | ACC Testing Majority voting | FNR Testing Majority voting |
|---|---|---|---|---|---|---|---|
| **Location 1 (test) Location 2 (training)** | 2 | 0.9890 | 0.0067 | 0.8605 (0.6916) | 0.0269 | 0.8875 (0.7422) | 0.0156 |
| | 4 | 0.9917 | 0.0033 | 0.8275 (0.7223) | 0.0121 | 0.8500 (0.7500) | 0 |
| | 6 | 0.9867 | 0.0078 | 0.7765 (0.7312) | 0.0425 | 0.8000 (0. 7500) | 0 |
| | 8 | 0.9480 | 0.0173 | 0.7200 (0.7200) | 0.1690 | 0.7875 (0.7875) | 0.0500 |
| | 10 | 0.9263 | 0.0675 | 0.6755 (0.6744) | 0.3350 | 0.7500 (0. 7552) | 0.2188 |
| **Location 2 (test) Location 1 (training)** | 2 | 0.9805 | 0.0025 | 0.8750 (0.7987) | 0.0742 | 0.8750 (0.7969) | 0.0729 |
| | 4 | 0.9630 | 0.0050 | 0.8750 (0.8334) | 0.0638 | 0.8917 (0.8452) | 0.0476 |
| | 6 | 0.9350 | 0.0108 | 0.8923 (0.8900) | 0.0994 | 0.9417 (0.9514) | 0.0556 |
| | 8 | 0.9185 | 0.0360 | 0.8210 (0.8213) | 0.2813 | 0.8583 (0.8583) | 0.2167 |
| | 10 | 0.9160 | 0.1175 | 0.7323 (0.6794) | 0.5833 | 0.7333 (0. 6701) | 0.6458 |

Table 2**.** Results of classification for the two sessions in terms of ACC and FNR in training, in testing, and after the implementation of majority voting. Numbers in brackets represent the balanced accuracy values computed as the average value between True Positive Rate (TPR) and True Negative Rate (TNR).

## SUPPLEMENTARY MATERIAL

# Optical detection of Aflatoxins B in grained almonds using fluorescence spectroscopy and machine learning algorithms

F. R. Bertani[a], L. Businaro[a], L. Gambacorta[b], A.Mencattini[c] , D. Brenda[c], D. Di Giuseppe[c], A. De Ninno[a], M. Solfrizzo[b], E. Martinelli[c], A. Gerardino[a]

[a]Consiglio Nazionale delle Ricerche, Istituto di Fotonica e Nanotecnologie, via Cineto Romano 42, 00156, Roma, Italia

[b] Consiglio Nazionale delle Ricerche, Istituto di Scienze delle Produzioni Alimentari, via Amendola, 122/O - 70126 Bari, Italia

[c]Department of Electronic Engineering, University of Rome Tor Vergata, via del Politecnico 1, 00133, Roma, Italia

e-mail: francesca.bertani@ifn.cnr.it

In this section, we show the Principal Component Analysis (PCA) results of the dataset used for the classification of Aflatoxins B contamination levels. Figure S1 shows the first two principal components of the dataset grouped by locations (Fig. S1-a), by days (Fig. S1-b, days are labelled as 1, 2, and 3 for the two locations), and by contamination levels (Fig. S1-c).

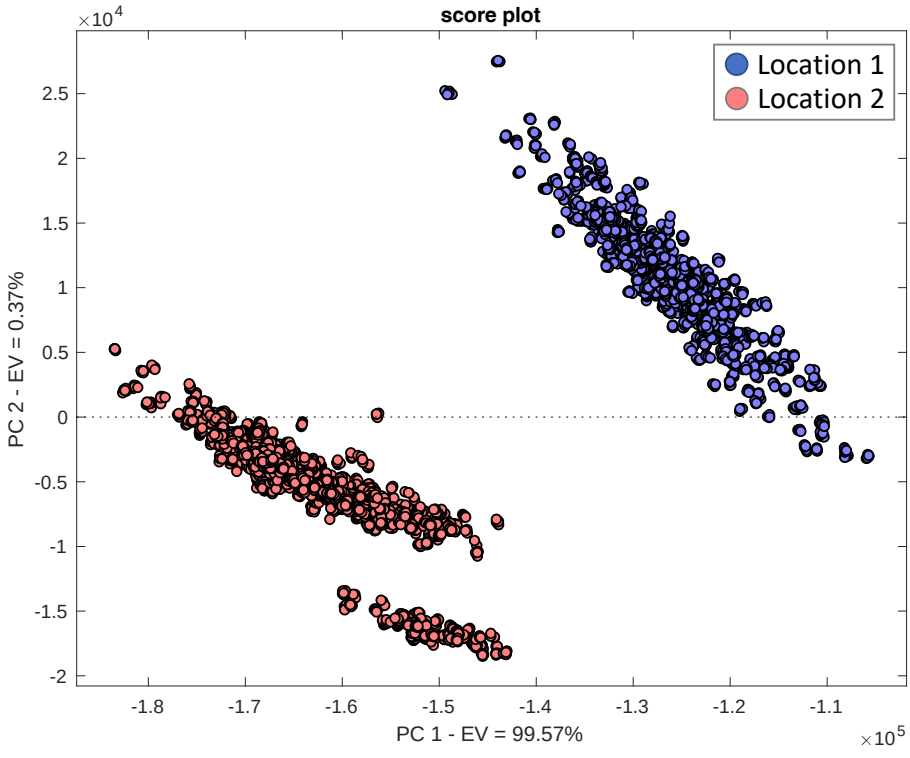


(a)

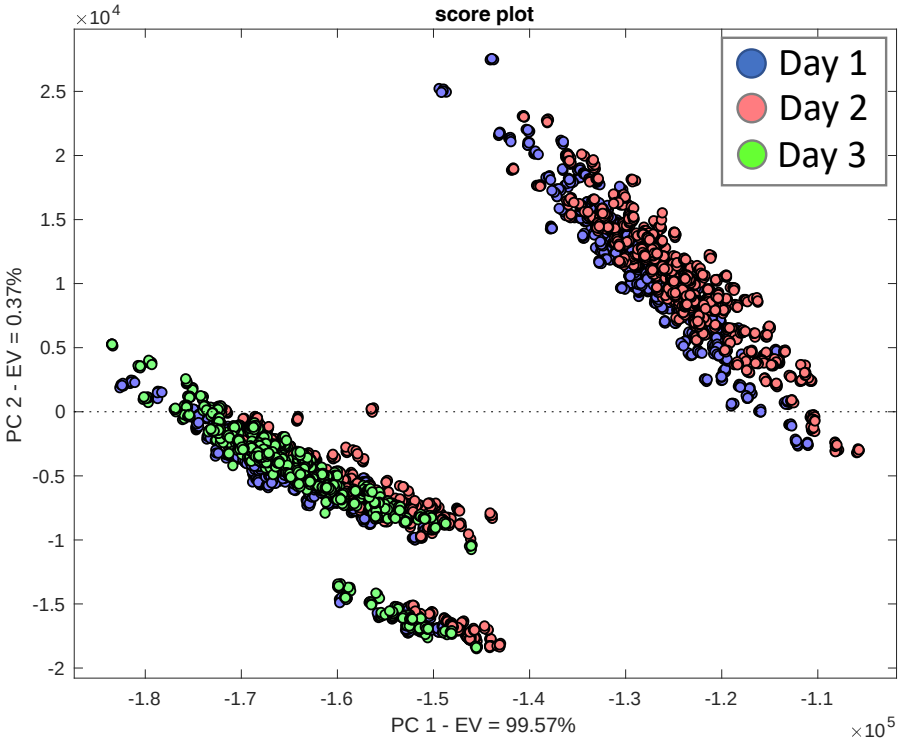


(b)

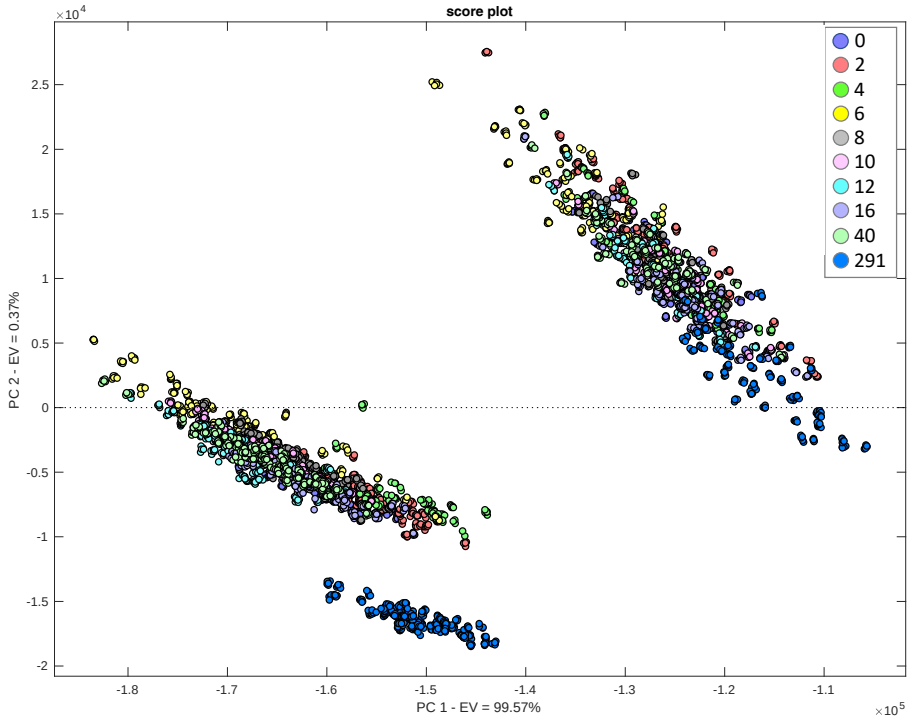


c)

**Figure S1.** Principal component analysis (PCA) results of the dataset in the PC1 and PC2 components. (a) scores are grouped according to location (blue is location 1 and red is location 2, class 1 and 2 respectively). (b) scores are grouped according to days of acquisition (blue and red dots are days 1 and 2 for both the locations, whereas green dots represent day 3 for location 2). (c) scores are grouped according to the contamination levels from 0 (class 1) to 291 ng/g (class 10).

Results visualized support the fact that there is a strong heterogeneity between the two measurement sessions (locations 1 and 2) (Fig. S1-a). In addition, it is also evident that variation over days is not so strong within the same location (Fig. S1-b). Anyway, is it also remarkable that there is an unequal variation over contamination levels in the two locations, with a more evident separation of high contamination levels (291 ng/g, labelled as class 10) in location 2 where it is expected that the measurement protocol had been further optimized and improved with respect to the location 1 where contaminations levels were more confused.